ACS APPLIED MATERIALS & INTERFACES

Research Article

www.acsami.org

Improvement of Stability for Small Molecule Organic Solar Cells by Suppressing the Trap Mediated Recombination

Xia Hao,[*,†] Shenghao Wang,[*,†,∥] Takeaki Sakurai,[†,‡] Shigeru Masuda,[§] and Katsuhiro Akimoto[†]

[†]Institute of Applied Physics, University of Tsukuba, Tsukuba, Ibaraki 305-8573, Japan

[‡]PRESTO, Japan Science and Technology Agency (JST), Kawaguchi, Saitama 332-0012, Japan

[§]Department of Basic Science, Graduate School of Arts and Sciences, The University of Tokyo, Komaba, Meguro, Tokyo 153-8902, Japan

Supporting Information

ABSTRACT: To understand the degradation mechanism of organic solar cells (OSCs), the charge dynamics of conventional and inverted planar heterojunction OSCs based on boron subthalocyanine chloride (SubPc) and fullerene (C_{60}) with identical buffers during the air exposure were investigated. The results of light intensity dependent open circuit voltage show that the bimolecular recombination is dominated in the fresh devices, regardless of the device structure. The appearance of transient peak in photocurrent after turn-on and the light intensity independent turn-off traces in transient photocurrent suggest that the rapid degradation of conventional device is due to the energy loss originated from the aggravated trap mediated recombination. In contrast, the half-lifetime of inverted device is ∼25 times longer than the conventional one. The improvement of stability is ascribed to the decrease of the trap generation possibility and the suppression of trap mediated recombination in the case of inverted structure, where the penetration of oxygen and water through buffer layer is avoided.

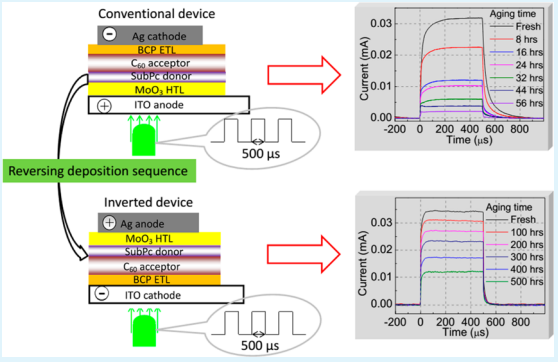

KEYWORDS: *organic solar cells (OSCs), recombination, charge dynamics, transient photocurrent (TPC), stability*

1. INTRODUCTION

Organic solar cells (OSCs) have attracted great interest and achieved progress due to the advantages of light weight, flexibility, and potential low cost for large area fabrication.[1−9] Although the power conversion efficiency (PCE) has been improved greatly in the past decade, the short lifetime of OSCs hinders the residential application. It is generally accepted that the device performance degrades fast when it is exposed to oxygen and/or humid environment. The possible reasons for the fast degradation are the chemical and physical changes of the active layers, the instability of interfaces and the oxidation of electrodes.[10,11] Even though many studies have been done to improve the lifetime of OSCs by inserting an air-stable buffer layer (e.g., TiO_x,[12] ZnO,[13] poly(3,4-ethylenedioxythiophene):poly(styrene sulfonic acid) (PEDOT:PSS),[14] graphene oxide (GO),[15] and polymerized fluorocarbon film (CF_x)[16]) or by using a high work function metal electrode to avoid the degradation, the physical mechanism during the degradation process (i.e., charge dynamics) is not yet understood well. For example, by utilizing a different buffer layer, the interfacial properties between active/buffer/electrode layers may change, resulting in different properties for charge transfer at interfaces. Moreover, the morphology of the active layer may change when it is deposited on a different buffer layer, since the morphological properties are dependent on the properties of underneath layer (i.e., surface energy, wettability, and hydrophilicity/hydrophobicity). In this case, the changes of interface properties and morphological properties bring complexity to illustrate the deep mechanism during the degradation.

The study of both conventional structure and inverted structure OSCs with the identical constituted layers is very beneficial to reveal the device physics during the degradation because the effects of interface change and morphology change will be minimized. In this work, we investigated the charge dynamics of small molecule OSCs during the degradation by employing the same buffer layers, namely, bathocuproine ($C_{26}H_{20}N_2$, BCP) and MoO_3, into the conventional structure OSC and inverted structure OSC. In both devices, MoO_3 and BCP act as hole transport layer (HTL) and electron transport layer (ETL), respectively.

Transient techniques such as charge extraction by linearly increasing voltage (CELIV),[17] ultrafast transient photovoltage, time-of-flight (TOF),[18] and transient absorption spectroscopy (TAS)[19] can provide direct information regarding the charge transport and recombination dynamics to distinguish the

Received: May 19, 2015
Accepted: August 11, 2015
Published: August 11, 2015

DOI: 10.1021/acsami.5b04334
ACS Appl. Mater. Interfaces 2015, 7, 18379−18386

energy loss mechanisms. However, these approaches require rigid laser pulse, which is not only far away from the real operating conditions of device, but also would induce damage to the interface or composed materials. Transient photocurrent (TPC) measurement is quite preferable to acquire the charge behavior related information under the real device operating conditions. In TPC measurement, the information on the buildup of traps, charge transportation, and recombination dynamics can be obtained by studying the responses of photocurrent of OSCs to square-pulsed optical excitation. The TPC measurement has been used to investigate the charge trapping and recombination dynamics of bulk-hetrojunction OSCs,[20−24] but little work was carried out on the small molecule planar OSCs, where they may have different charge dynamic properties. In this work, the charge dynamic behaviors during the degradation for small molecule planar OSCs based on boron subthalocyanine chloride (SubPc) and fullerene (C_{60}) was investigated by TPC measurement. The results show that, in the conventional device, rapid degradation was caused by the aggravated trap mediated recombination, which originated from the degradation of BCP and C_{60} layers. The device lifetime was effectively improved by orienting the device structure in a way that reduces the penetration of oxygen and water. The reason for the improvement of the stability is ascribed to the decrease of trap generation possibility and the effective suppression of trap mediated recombination by well protecting C_{60} layer and BCP layer in the inverted structure.

2. EXPERIMENTAL STUDIES

The devices were prepared in a molecular beam epitaxy system by evaporating the materials in a vacuum chamber. The difference between the conventional and inverted devices is the opposite deposition sequence of the layers. The structures of conventional device and inverted device are illustrated in Figure 1. The thickness of

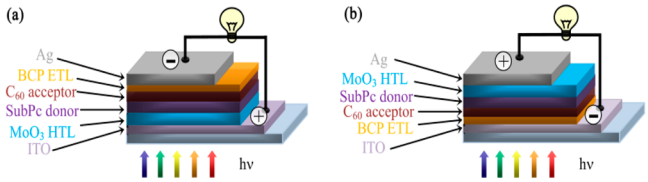

Figure 1. Illustrations of (a) the conventional structure OSC and (b) the inverted structure OSC.

layers for MoO_3, SubPc, C_{60}, BCP, and Ag are 25, 15, 50, 10, and 100 nm, respectively. In the conventional device, the indium tin oxide (ITO) and Ag acted as anode and cathode, respectively, whereas cathode and anode in the inverted structure device. The details for device fabrication can be seen elsewhere.[25] In order to characterize the degradation properties of OSCs, the unencapsulated devices were exposed to ambient air with a temperature of 25 °C and humidity of 50%. Except for carrying out the illuminated measurements, the devices were kept in the dark. The current density−voltage (J−V) characteristics were measured with a J−V source meter (Advantest R6245) under illumination with a light intensity of 100 mW/cm^2 at AM 1.5 G spectrum. For the TPC measurements, a high brightness 525 nm light-emitting diode (Kingbright L-7104VGC-H) was driven by a pulse generator (Agilent 33220A) to generate a square-pulse optical excitation. The rise and fall time of light was measured to be less than 100 ns by a Si biased photo detector (THORLABS DET10A/M). The frequency of 1 kHz and pulse width of 500 μs were chosen. The pulsed light intensity, calibrated by an optical power meter (THORLABS PM100D), was varied by adjusting the bias applied on the light-emitting diode. Signals of photocurrent were recorded by using a digital oscilloscope (Agilent DSO-X-2024A, input impendence of 1 MΩ) to measure the voltage drop across an extra 50 Ω resistance in series to the device.

3. RESULTS AND DISCUSSION

The surface morphologies of active materials play a very important role in the device performance, because they considerably affect the charge separation. A corrugated nanostructure is necessary to form interdigitated donor−acceptor interface.[26] We examined the morphologies of donor (SubPc) and acceptor (C_{60}) for the conventional structure and inverted structure. The AFM images of SubPc thin films (15 nm) deposited on ITO/MoO_3 and ITO/BCP/C_{60} stack layers, corresponding to the conventional structure and inverted structure, respectively, are presented in Figure 2a,b. The root-mean-square (RMS) roughnesses of SubPc films deposited on ITO/MoO_3 and ITO/BCP/C_{60} are 3.5 and 4.7 nm, respectively. The SubPc films show similar surface morphologies from the viewpoint of forming corrugated structure with little difference of the roughness. Figure 2c,d show the AFM images of C_{60} layers deposited on ITO/MoO_3/SubPc and ITO/BCP stack layers, corresponding to the conventional structure and the inverted structure, respectively. We can see that the C_{60} layer deposited on ITO/BCP has much smoother morphology with RMS roughness of 1.8 nm, whereas the C_{60} layer deposited on ITO/MoO_3/SubPc stack layers shows a rough surface with RMS roughness of 3.3 nm. Even though the morphological properties of SubPc in the conventional and inverted structures are similar, the morphological properties of C_{60} layer in the two device structures are different. The smoother C_{60} layer deposited on BCP in the inverted structure makes it possible to form a good interface contact between acceptor and donor,[27] resulting in effective charge separation at C_{60}/SubPc interface.

Figure 3 shows the J−V characteristics for both devices as a function of aging time. The photovoltaic parameters of conventional and inverted devices during the aging process were summarized in Table 1. The fresh conventional device shows a short circuit current density (J_{SC}) of 3.86 mA/cm^2, open circuit voltage (V_{OC}) of 1.02 V, fill factor (FF) of 0.49, and PCE of 1.93%. With the increased exposure time, the device performance becomes seriously worse. The reductions of J_{SC}, V_{OC}, and FF are all responsible for the degradation of device performance. From the variation of PCE during the degradation, as shown in Figure 3c, we can see that it only took 20 h for the PCE to decay to 50% of its initial value. After being exposed for 44 h, the device degraded heavily, only with a low PCE of 0.29%. On the other hand, the inverted device fabricated by reversing the deposition sequence of all the functional layers shows much better stability. Figure 3b depicts the J−V characteristics of inverted device as a function of aging time. The fresh inverted device shows a J_{SC} of 4.71 mA/cm^2, V_{OC} of 0.99 V, FF of 0.41, and PCE of 1.91%. The J_{SC} of the inverted device is higher than that of the conventional device, which is consistent with the morphological properties of donor/acceptor interface as discussed above. Note that S-kinks involve into the J−V curves of inverted device, which were caused by the charge accumulation at C_{60}/BCP interface.[28] The S-shaped J−V curve lowered the FF of the inverted device. It should be noticed that the S-shaped J−V curve is only dependent on the structure of the device, whereas it is independent of the aging time. This indicates that the change of electronic properties (i.e., energy level alignment) of the C_{60}/BCP interface is negligible. The series resistance (R_S) was

DOI: 10.1021/acsami.5b04334
ACS Appl. Mater. Interfaces 2015, 7, 18379−18386

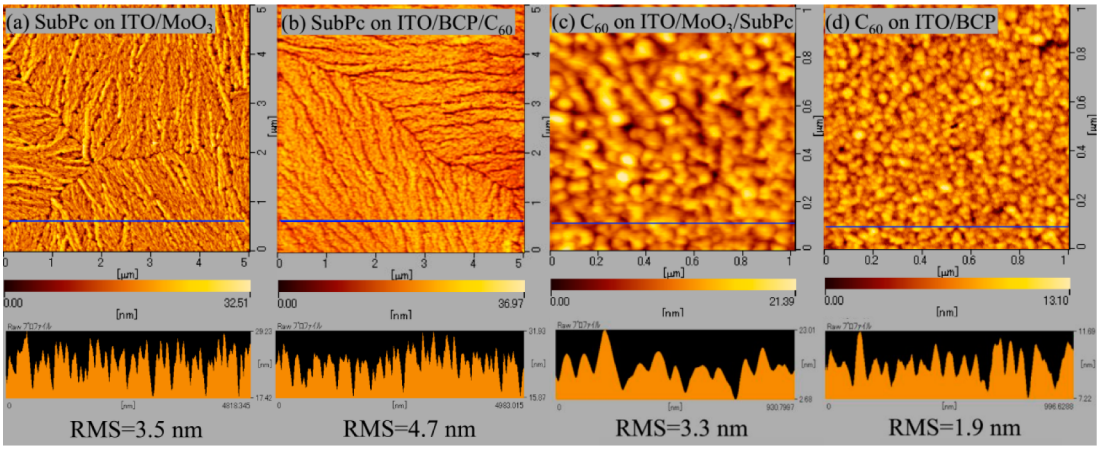

Figure 2. AFM images of 15 nm SubPc deposited on (a) ITO/MoO_3 (30 nm) and (b) ITO/BCP (10 nm)/C_{60} (50 nm), taken with scan area of 5 × 5 μm^2; AFM images of 50 nm C_{60} deposited on (c) ITO/MoO_3 (30 nm)/SubPc (15 nm), and (d) ITO/BCP (10 nm), taken with scan area of 1 × 1 μm^2.

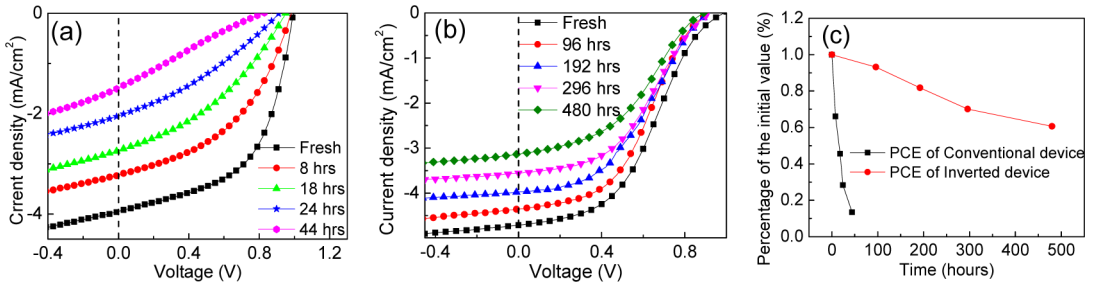

Figure 3. *J*–*V* curves of (a) the conventional device and (b) the inverted device as a function of aging time. The variations of normalized PCEs during degradation are shown in part c.

Table 1. Photovoltaic Parameters of Conventional and Inverted Devices with Increased Aging Time

aged time (h)	J_{SC} (mA/cm^2)	V_{OC} (V)	FF	PCE (%)	R_S (Ω cm^2)
Conventional Device					
0	3.86	1.02	0.49	1.93	44
8	3.22	0.99	0.40	1.28	82
18	2.70	0.92	0.33	0.89	145
24	2.07	0.90	0.29	0.54	496
44	1.49	0.82	0.24	0.29	847
Inverted Device					
0	4.71	0.99	0.41	1.91	380
96	4.35	0.98	0.40	1.71	332
192	4.01	0.97	0.40	1.52	266
296	3.58	0.95	0.41	1.42	239
480	3.14	0.91	0.40	1.14	388

calculated from the inverse of the slope of the tangential line of the *J*–*V* curve at V_{OC}.[29] The R_S of the fresh inverted device is 380 Ω cm^2, which is much higher than that of the fresh conventional device (44 Ω cm^2). The larger R_S of inverted device is caused by the low conductivity of intrinsic BCP,[30] whereas the interaction between Ag and BCP, which occurred during the Ag deposition for the conventional device, can increase the conductivity of BCP and hence result in the smaller R_S.[28,30−32]

For the conventional devices, as shown in Table 1, R_S increases rapidly from 44 (for the fresh device) to 847 Ω cm^2 (for the device aged for 44 h). The increase of R_S is the main cause of the deterioration of J_{SC}. It is generally agreed that oxygen and water can penetrate into the inner layer through metal boundary and pinholes.[33,34] This can lead to BCP recrystallization and then produce pinhole channels for oxygen/water penetrating into C_{60} (see Figures S1 and S2, Supporting Information). It has been reported that C_{60} is very sensitive to oxygen and water, which would induce the decrease of carrier mobility and the traps for electrons in the C_{60} layer.[35,36] In the conventional OSCs, the C_{60} is adjacent to the top metal cathode, suggesting that it is vulnerable to the air atmosphere. Thus, the quick increase of R_S can be ascribed to the carrier mobility decrease of C_{60} layer with increasing exposing time. As a result, the J_{SC} of the conventional device decreases considerably with aging time (from 3.86 mA/cm^2 for the fresh device to 1.49 mA/cm^2 for the aged 44 h device). The traps in the C_{60} layer can lead to the recombination at the SubPc/C_{60} interface. Here it should be commented that the recombination may be very different from the bulk heterojunction (BHJ) OSCs (e.g., polymer OSCs), because both interfacial recombination and bulk recombination can be involved in the BHJ OSCs.[37−40] After degradation, the V_{OC} of the conventional device also decreased rapidly from 1.02 to 0.83 V. The decrease of V_{OC} suggests that the recombination may be aggravated during the degradation. On the contrary, MoO_3 is regarded as a very stable material which can serve as a protective layer to avoid undesirable physical and chemical reactions between electrodes and other layers (i.e., BCP and C_{60}) induced by the penetrated oxygen and water,[41,42] and hence prolong the lifetime expectancy of the device. As compared with the conventional device, the decrease of J_{SC} (~33% decrease during 480 h aging) is considerably suppressed

DOI: 10.1021/acsami.5b04334
ACS Appl. Mater. Interfaces 2015, 7, 18379−18386

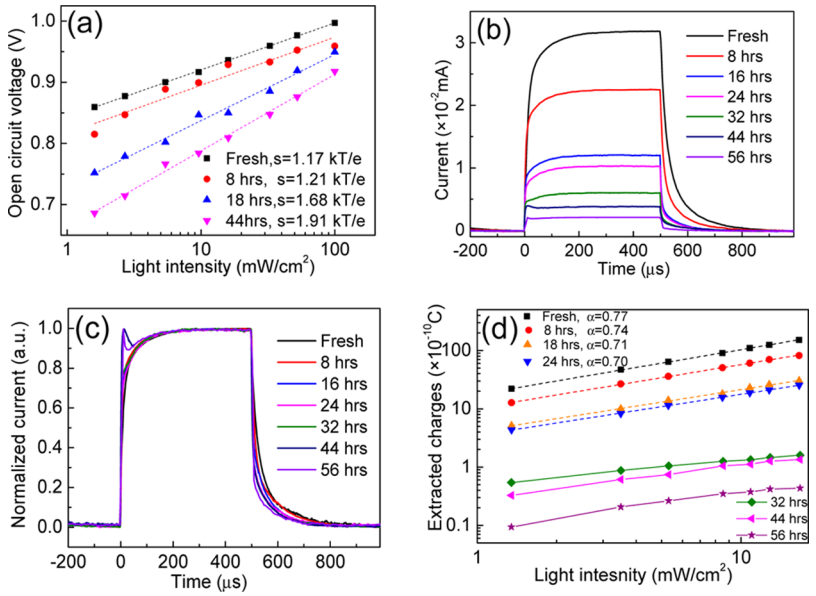

Figure 4. Characteristics of conventional device as a function of aging time: (a) light intensity dependent V_{OC}, (b) the absolute transient photocurrent, (c) the normalized transient photocurrent, and (d) the amount of extracted charge vs light intensity. The symbols represent the experimental data and the dotted lines are for the fitting. The connecting solid lines in part d show the complex relationship between extracted charge and light intensity.

in the inverted device, whereas the J_{SC} decreased by 61% only during 44 h aging time for the conventional device. The V_{OC} of the inverted device only slightly decreased during the aging from fresh to 480 h. It may be related to the suppression of recombination.

The trap-assisted recombination is a two-step process: (1) a new energy level is created inside the energy band gap by a trap state; and (2) this new energy level captures a charge carrier that subsequently recombines with an opposite charged carrier due to their Coulomb interaction.[43] The impacts of trap-assisted recombination could be revealed by the light intensity dependence of V_{OC}. The V_{OC} and light intensity (I) are correlated by the following expression:[40]

$$V_{OC} = \frac{1}{e}(E_{LUMO}^{C60} - E_{HOMO}^{SubPc} - \Delta) - \frac{kT}{e}\ln\left(\frac{n_e n_h}{N_c^2}\right) \quad (1)$$

Here e is the elementary charge, E_{LUMO}^{C60} is the lowest unoccupied molecular orbital (LUMO) level of C_{60}, E_{HOMO}^{SubPc} is the highest occupied molecular orbital (HOMO) of SubPc, Δ represents the relative small band tailing to energy below the LUMO of acceptor, k is the Boltzmann constant, T is the temperature in Kelvin, N_C is the effective density of states, and n_e and n_h are the electron and hole densities, respectively. In the case of bimolecular recombination, $n_e n_h = G/\gamma$,[44] in which γ is the bimolecular recombination constant and G is the generation rate of polaron pairs. Considering that G is the only term which is proportional to the light intensity (I), the V_{OC} could be given by[40]

$$V_{OC} \propto \left(\frac{kT}{e}\right)\ln(I) + \text{const.} \quad (2)$$

This formula implies that the slope of V_{OC} versus $\ln(I)$ is equal to kT/e for bimolecular recombination. For the trap-assisted recombination, due to the n_e and n_h at open circuit, would each be proportional to light intensity, a stronger dependence of V_{OC} on light intensity is expected, namely, with a slope of $2kT/e$ for V_{OC} versus $\ln(I)$.[40] Figure 4a depicts the V_{OC} versus $\ln(I)$ relationship for fresh, aged for 8, 18, and 44 h of conventional device. With the increase of aging time, a gradual increase in the slope (denoted as s in the figure) was witnessed, from $1.17kT/e$ for the fresh device to $1.91kT/e$ for the heavily degraded one (44 h). This suggests that the trap-assisted recombination was aggravated during the air-exposure process. This is also consistent with the decrease of V_{OC} with increasing the aging time.

The aggravation of recombination during the degradation process can be further verified by the TPC measurement. Figure 4b,c present the turn-on and turn-off dynamics of TPC as a function of aging time, with pulse light intensity of 14.3 mW/cm^2. Generally, the transient photocurrent signal of the fresh device is composed of the following: a fast rise followed by a slow increase until reaching the equilibrium after turn-on and a fast decay with a gradual decreased positive tail after turn-off. However, the TPC signals obviously changed with the increased aging time. As shown in Figure 4b, for the turn-on behavior, the intensity of the TPC decreases along with the aging time, which is due to the trap-induced reduction in charge generation efficiency.[45] In addition, a transient peak in the photocurrent after turn-on in the TPC emerged with the increased exposing time. This feature can be clearly discerned when the curves are normalized in Figure 4c. The transient peak corresponds to the trap-assisted recombination.[46] As for the turn-off dynamics, a fast decay followed by a long-lived positive tail suggests the slow detrapping process of the trapped charges in the aged device. The aggravated recombination may affect the charge extraction in the device. The amount of extracted charge in the conventional device was calculated by integrating the current after turn-off in the TPC transients. The amount of extracted charge (Q_e) versus light intensity (I) as a function of aging time for conventional device was displayed in Figure 4d. The extracted charge in device aged for less than 24 h can be fitted by $Q_e \propto I^{\alpha}$, yielding α value. Compared to the power law exponents in J_{SC} versus I (see Figure S3, Supporting

DOI: 10.1021/acsami.5b04334
ACS Appl. Mater. Interfaces 2015, 7, 18379−18386

Information), the lower slope values for plot of Q_e versus I suggests that the charge extraction is more sensitive to recombination than photocurrent. After aging for 24 h, with increased aging time, the plot of Q_e versus I exhibits a more complex relationship, which cannot be fitted by the power law anymore. The possible reasons for this complex dependence of Q_e versus I for heavily aged conventional device could be ascribed to the slow detrapping of trapped charges or the recombination loss after turn-off.

The recombination effect in the degraded device could be further clarified by observing the photocurrent transients as a function of incident light intensity. Figure 5 presents the short

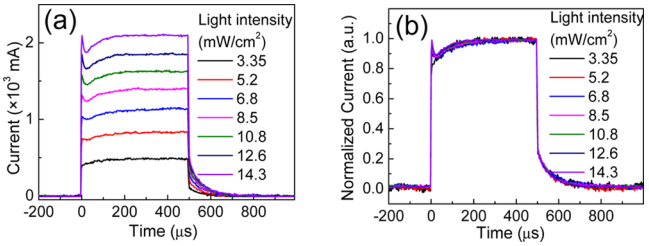

Figure 5. Light intensity dependence of photocurrent transients for the conventional device after aged 56 h: (a) for the absolute traces and (b) for the normalized traces.

circuit photocurrent response to the pulsed light for the heavily aged device. From Figure 5a, we can see that the TPC signal displays fast turn-on and turn-off dynamics with a quasi-rectangular shape at low intensities. With the increase of pulse intensity, a transient peak in the photocurrent after turn-on emerges and becomes prominent. The turn-on and turn-off features can be more clearly discerned in the normalized traces in Figure 5b. For the turn-on behavior, the population of the photogenerated charges is limited under low pulse intensity, so the effect of recombination is minimal. In this case, the TPC only reflects the trapping/detrapping process. However, with increasing pulse intensity, the photogenerated charge density becomes higher, and the population of the trapped charges increases until reaching the equilibrium. The free carriers were swept out, and some of them were then recombined. Therefore, the transient peak in the photocurrent after turn-on appeared under high light intensities is also an evidence of trap-assisted recombination.

On the other hand, the long tail following the sharp decrease in the turn-off behavior suggests that the charges are still extracted for ~300 μs due to detrapping. For device with traps that were not yet involved in obvious trap mediated recombination, owing to the slow detrapping process, the transient photocurrent after turn-off is expected to be light intensity dependent. However, except for the presence of transient peak in the photocurrent after turn-on, the traces in the turn-off behaviors in normalized TPC in Figure 5b are overlapped under various light intensities. With the presence of trap, the charge trapping will increase the total charge density in the degraded device. The increased charge density will then result in an increased possibility of bimolecular recombination between free electrons and holes at the donor/acceptor interface. Thus, the charge trapping not only results in trap-assisted recombination, but also induces much more severe bimolecular recombination. Therefore, we concluded that the light intensity independent turn-off behavior is a reflection of a combination of charge detrapping and trap mediated recombination.

In comparison, the charge dynamic properties for inverted device are also shown. Figure 6a shows the V_{OC} dependence upon light intensity. With the increased aging time, the slope of V_{OC} versus ln(I) for inverted device also increased gradually while at a much slower rate as compared with the conventional one. For the device of a fresh one and the one aged for 96 h, the predominant recombination is the bimolecular recombination with s = 1.08kT/e and 1.10kT/e, respectively. Further extending the aging time, the s value gradually increased. For the inverted device aged for 480 h, the s equals to 1.42 kT/e, suggesting that the recombination at open circuit is a combination of bimolecular recombination and trap-assisted recombination. On the contrary, the heavily aged conventional

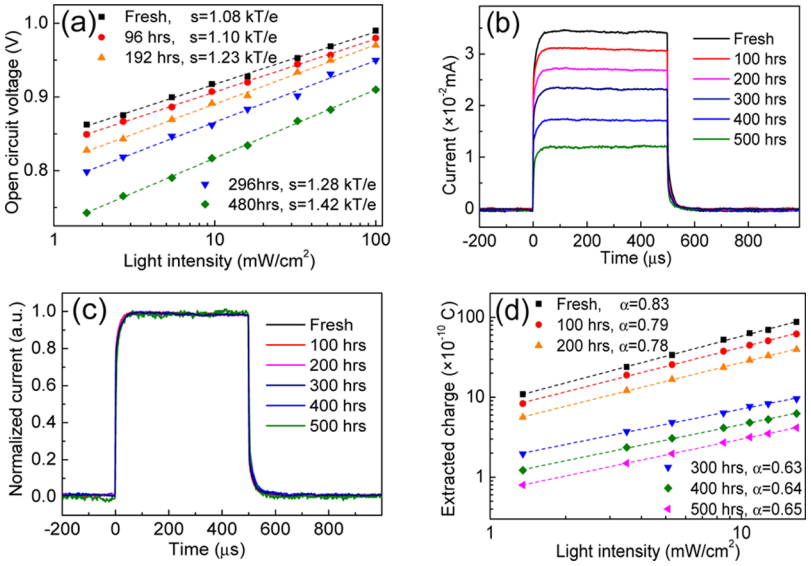

Figure 6. Characteristics of inverted device as a function of aging time: (a) light intensity dependent V_{OC}, (b) the absolute transient photocurrent, (c) the normalized photocurrent, and (d) the amount of extracted charge vs light intensity. The symbols represent the experimental data, and the dotted lines are for the fitting.

DOI: 10.1021/acsami.5b04334
ACS Appl. Mater. Interfaces 2015, 7, 18379−18386

device (44 h) possesses a much larger s value ($1.91kT/e$), indicating the dominant trap-assisted recombination. The weaker dependence of V_{OC} on the light intensity during the degradation for the inverted device clearly suggests a successful suppression of trap-assisted recombination in the inverted device. Then the TPC measurement was employed to the inverted device to verify this suppression effect.

Ignoring bimolecular recombination at high intensity, for trap-free charge transport and fast electron−hole pair separation, the turn-on behavior is primarily determined by the charge mobility and independent of pulse intensity. Figure 6b presents the TPC of inverted device as a function of aging time, with pulse light intensity of 14.3 mW/cm^2. The photocurrent transient increases rapidly to the plateau region, and decreases fast after turn-off. As compared to the conventional device, the turn-on and turn-off dynamics of the inverted device are much faster, indicating fast transport of the free carriers in the inverted device. With the increased aging time, the intensity of the TPC decreases, which coincides with the decreased J_{SC}. This TPC intensity reduction in the aged devices may due to the trap-induced reduction in charge generation efficiency. Additionally, there is little change in the TPC shape under various exposing time in the inverted device, whereas drastic change of TPC signal in the conventional device as aforementioned. From the normalized TPC traces in Figure 6c, we can see that the inverted device shows no dependence on aging time in 500 h. This suggests that the charge behaviors are not significantly affected by the air exposure for an inverted device. To get a full comparison with a conventional device, Q_e plotted against light intensity as a function of aging time for inverted device is also shown in Figure 6d. The light intensity dependent photocurrent for the inverted device is shown in Figure S4 (Supporting Information), the slope of $J_{SC} \propto I^{\alpha}$ plot shows a slight decrease with the increased aging time, suggesting that the charge separation was not obviously affected by the air exposure. As for the charge extraction, even if the device was aged for 500 h, the plot of Q_e versus I could be well-fit by the power law. Therefore, for the inverted device, the charge separation was not obviously affected in 500 h air exposure. Also, the slightly degraded PCE after 500 h of aging time could be ascribed to the decreased efficiency of charge extraction.

To get further insight into the charge behaviors after aging, the TPC results for the inverted device aged for 500 h as a function of light intensity are shown in Figure 7a,b. We can see that, at low pulse intensities, the TPC shows slower dynamics, which are related to the time taken for the trapping/detrapping processes to reach steady state after turn-on, or the time taken for charge detrapping after turn-off. In addition, not like the degraded conventional device, the photocurrent transients of inverted device aged for 500 h are dependent on the pulse intensity, which can be clearly observed in Figure 7b. Such pulse intensity dependent behavior suggests the trapping and detrapping effects but no evident trap mediated recombination. Importantly, although the magnitude of TPC decreases in the aged device, there is no transient peak in the photocurrent after turn-on, even at high light intensities. This suggests that the trap-assisted recombination is greatly suppressed, which is consistent with the small change of V_{OC} during 480 h aging: from 0.99 to 0.91 V. Therefore, the stability is significantly improved for the inverted device.

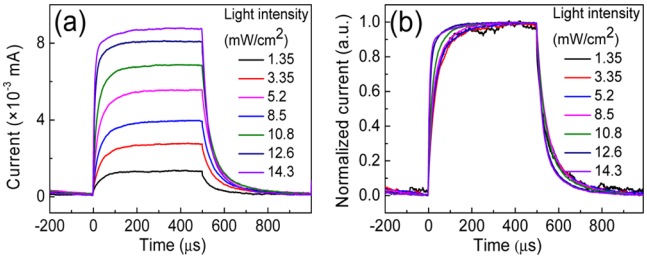

Figure 7. Light intensity dependence of photocurrent transients for the inverted device after aged 500 h: (a) for the absolute traces and (b) for the normalized traces.

4. CONCLUSION

We investigated the charge dynamics of C_{60}-based planar OSCs with conventional and inverted structures during the degradation in air ambient. For the conventional device, it only takes 20 h for the PCE to decay to 50% of its initial value. The rapid degradation is caused by the deterioration of BCP and the formation of traps in the C_{60} layer. The TPC results show that a transient peak in the photocurrent after turn-on comes out with increasing the exposing time. In addition, the turn-off dynamics in the TPC is independent of the pulse intensity during the degradation. These features are ascribed to the aggravation of trap mediated recombination with increasing the aging time in the conventional device. In contrast, the stability of the inverted device was improved greatly with the half-lifetime of ∼25 times longer than the conventional device. The absence of transient peak in the photocurrent after turn-on and pulse intensity dependent turn-off traces in the TPC imply that the trap mediated recombination was significantly suppressed in the case of inverted structure, where C_{60} layer and BCP layer are well-protected by air-stable MoO_3 layer to avoid the penetration of oxygen and water. This study demonstrates the recombination mechanism of small molecular OSC during the degradation, and provides insight into further understand the degradation mechanism and further improve the long-term stability of OSCs.

■ ASSOCIATED CONTENT

Supporting Information

Optical microscopy images of BCP film featuring the BCP recrystallization; AFM images of BCP film before and after air exposure featuring the presence of pinholes; the plots of J_{SC} *vs* I for conventional device and inverted device as a function of aging time. The Supporting Information is available free of charge on the ACS Publications website at DOI: 10.1021/acsami.5b04334.

(PDF)

■ AUTHOR INFORMATION

Corresponding Authors

*E-mail: hao.xia0808@gmail.com.
*E-mail: wsh8511@gmail.com.

Present Address

[‖]Okinawa Institute of Science and Technology Graduate University (OIST), Onna, Okinawa 904-0495, Japan.

Notes

The authors declare no competing financial interest.

DOI: 10.1021/acsami.5b04334
ACS Appl. Mater. Interfaces 2015, 7, 18379−18386

■ ACKNOWLEDGMENTS

This work is partially supported by the Marubun Research Promotion Foundation, Japan.

■ ABBREVIATIONS

OSC, organic solar cell
PCE, power conversion efficiency
PEDOT:PSS, poly(3,4-ethylenedioxythiophene):poly(styrene sulfonic acid)
GO, graphene oxide
CF_x, polymerized fluorocarbon film
BCP, bathocuproine
HTL, hole transport layer
ETL, electron transport layer
CELIV, charge extraction by linearly increasing voltage
TOF, time-of-flight
TAS, transient absorption spectroscopy
TPC, transient photocurrent
SubPc, boron subthalocyanine chloride
C_{60}, fullerene
ITO, indium tin oxide
$J-V$, current density−voltage
RMS, root-mean-square
J_{SC}, short circuit current
V_{OC}, open circuit voltage
FF, fill factor
R_S, series resistance

■ REFERENCES

(1) Tang, C. W. Two-Layer Organic Photovoltaic Cell. *Appl. Phys. Lett.* **1986**, *48*, 183−185.
(2) Wu, Y.; Zhang, W.; Li, X.; Min, C.; Jiu, T.; Zhu, Y.; Dai, N.; Fang, J. Solution-Processed Hybrid Cathode Interlayer for Inverted Organic Solar Cells. *ACS Appl. Mater. Interfaces* **2013**, *5*, 10428−10432.
(3) Chi, C.-Y.; Chen, M.-C.; Liaw, D.-J.; Wu, H.-Y.; Huang, Y.-C.; Tai, Y. A Bifunctional Copolymer Additive to Utilize Photoenergy Transfer and to Improve Hole Mobility for Organic Ternary Bulk-Heterojunction Solar Cell. *ACS Appl. Mater. Interfaces* **2014**, *6*, 12119−12125.
(4) Schubert, S.; Müller-Meskamp, L.; Leo, K. Unusually High Optical Transmission in Ca:Ag Blend Films: High-Performance Top Electrodes for Efficient Organic Solar Cells. *Adv. Funct. Mater.* **2014**, *24*, 6668−6676.
(5) Chen, J. D.; Zhou, L.; Ou, Q. D.; Li, Y. Q.; Shen, S.; Lee, S. T.; Tang, J. X. Enhanced Light Harvesting in Organic Solar Cells Featuring a Biomimetic Active Layer and a Self-Cleaning Antireflective Coating. *Adv. Energy Mater.* **2014**, *4*, 1301777.
(6) Xu, Z.-Q.; Yang, J.-P.; Sun, F.-Z.; Lee, S.-T.; Li, Y.-Q.; Tang, J.-X. Efficient Inverted Polymer Solar Cells Incorporating Doped Organic Electron Transporting Layer. *Org. Electron.* **2012**, *13*, 697−704.
(7) Wang, X.; Ho, J. W.; Yang, Q.; Tam, H. L.; Li, G. X.; Cheah, K. W.; Zhu, F. Performance Enhancement in Organic Photovoltaic Devices Using Plasma-Polymerized Fluorocarbon-Modified Ag Nanoparticles. *Org. Electron.* **2011**, *12*, 1943−1947.
(8) Liu, Y.; Qi, N.; Song, T.; Jia, M.; Xia, Z.; Yuan, Z.; Yuan, W.; Zhang, K.-Q.; Sun, B. Highly Flexible and Lightweight Organic Solar Cells on Biocompatible Silk Fibroin. *ACS Appl. Mater. Interfaces* **2014**, *6*, 20670−20675.
(9) Huang, W.; Gann, E.; Cheng, Y.-B.; McNeill, C. R. In-Depth Understanding of the Morphology-Performance Relationship in Polymer Solar Cells. *ACS Appl. Mater. Interfaces* **2015**, *7*, 14026−14034.
(10) Wang, X.; Xinxin Zhao, C.; Xu, G.; Chen, Z.-K.; Zhu, F. Degradation Mechanisms in Organic Solar Cells: Localized Moisture Encroachment and Cathode Reaction. *Sol. Energy Mater. Sol. Cells* **2012**, *104*, 1−6.
(11) Jørgensen, M.; Norrman, K.; Krebs, F. C. Stability/Degradation of Polymer Solar Cells. *Sol. Energy Mater. Sol. Cells* **2008**, *92*, 686−714.
(12) Chang, J.; Lin, Z.; Jiang, C.; Zhang, J.; Zhu, C.; Wu, J. Improve the Operational Stability of the Inverted Organic Solar Cells Using Bilayer Metal Oxide Structure. *ACS Appl. Mater. Interfaces* **2014**, *6*, 18861−18867.
(13) Kam, Z.; Wang, X. Z.; Zhang, J.; Wu, J. Elimination of Burn-in Open-Circuit Voltage Degradation by ZnO Surface Modification in Organic Solar Cells. *ACS Appl. Mater. Interfaces* **2015**, *7*, 1608−1615.
(14) Bovill, E.; Scarratt, N.; Griffin, J.; Yi, H.; Iraqi, A.; Buckley, A.; Kingsley, J.; Lidzey, D. The Role of the Hole-Extraction Layer in Determining the Operational Stability of a Polycarbazole: Fullerene Bulk-Heterojunction Photovoltaic Device. *Appl. Phys. Lett.* **2015**, *106*, 073301.
(15) Murray, I. P.; Lou, S. J.; Cote, L. J.; Loser, S.; Kadleck, C. J.; Xu, T.; Szarko, J. M.; Rolczynski, B. S.; Johns, J. E.; Huang, J. Graphene Oxide Interlayers for Robust, High-Efficiency Organic Photovoltaics. *J. Phys. Chem. Lett.* **2011**, *2*, 3006−3012.
(16) Lo, M. F.; Ng, T. W.; Lai, S.; Fung, M. K.; Lee, S. T.; Lee, C. S. Stability Enhancement in Organic Photovoltaic Device by Using Polymerized Fluorocarbon Anode Buffer Layer. *Appl. Phys. Lett.* **2011**, *99*, 033302.
(17) Tan, M. J.; Goh, W.-P.; Li, J.; Pundir, G.; Chellappan, V.; Chen, Z.-K. Charge Mobility and Recombination in a New Hole Transporting Polymer and Its Photovoltaic Blend. *ACS Appl. Mater. Interfaces* **2010**, *2*, 1414−1420.
(18) Chen, Y.; Peng, J.; Su, D.; Chen, X.; Liang, Z. Efficient and Balanced Charge Transport Revealed in Planar Perovskite Solar Cells. *ACS Appl. Mater. Interfaces* **2015**, *7*, 4471−4475.
(19) Zhang, B.; Yuan, H.; Zhang, X.; Huang, D.; Li, S.; Wang, M.; Shen, Y. Investigation of Regeneration Kinetics in Quantum-Dots-Sensitized Solar Cells with Scanning Electrochemical Microscopy. *ACS Appl. Mater. Interfaces* **2014**, *6*, 20913−20918.
(20) Tress, W.; Leo, K.; Riede, M. Influence of Hole-Transport Layers and Donor Materials on Open-Circuit Voltage and Shape of I-V Curves of Organic Solar Cells. *Adv. Funct. Mater.* **2011**, *21*, 2140−2149.
(21) Li, Z.; McNeill, C. R. Transient Photocurrent Measurements of PCDTBT: $PC_{70}BM$ and PCPDTBT: $PC_{70}BM$ Solar Cells: Evidence for Charge Trapping in Efficient Polymer/Fullerene Blends. *J. Appl. Phys.* **2011**, *109*, 074513.
(22) Qiao, X.; Zhao, C.; Chen, B.; Luan, L.; Hu, B. In-Situ Investigation of Interfacial Effects on Charge Accumulation and Extraction in Organic Solar Cells Based on Transient Photocurrent Studies. *Org. Electron.* **2014**, *15*, 1624−1630.
(23) Li, Z.; Gao, F.; Greenham, N. C.; McNeill, C. R. Comparison of the Operation of Polymer/Fullerene, Polymer/Polymer, and Polymer/Nanocrystal Solar Cells: A Transient Photocurrent and Photovoltage Study. *Adv. Funct. Mater.* **2011**, *21*, 1419−1431.
(24) Hwang, I.; McNeill, C. R.; Greenham, N. C. Drift-Diffusion Modeling of Photocurrent Transients in Bulk Heterojunction Solar Cells. *J. Appl. Phys.* **2009**, *106*, 094506.
(25) Hao, X.; Wang, S.; Sakurai, T.; Akimoto, K. Effect of Bathocuproine Buffer Layer in Small Molecule Organic Solar Cells with Inverted Structure. *Jpn. J. Appl. Phys.* **2015**, *54*, 04DK06.
(26) Kim, J.; Yim, S. Influence of Surface Morphology Evolution of SubPc Layers on the Performance of SubPc/C_{60} Organic Photovoltaic Cells. *Appl. Phys. Lett.* **2011**, *99*, 193303.
(27) Huang, J.; Yu, J.; Guan, Z.; Jiang, Y. Improvement in Open Circuit Voltage of Organic Solar Cells by Inserting a Thin Phosphorescent Iridium Complex Layer. *Appl. Phys. Lett.* **2010**, *97*, 143301.
(28) Hao, X.; Wang, S.; Fu, W.; Sakurai, T.; Masuda, S.; Akimoto, K. Novel Cathode Buffer Layer of Ag-Doped Bathocuproine for Small Molecule Organic Solar Cell with Inverted Structure. *Org. Electron.* **2014**, *15*, 1773−1779.
(29) Ichikawa, M.; Suto, E.; Jeon, H.-G.; Taniguchi, Y. Sensitization of Organic Photovoltaic Cells Based on Interlayer Excitation Energy Transfer. *Org. Electron.* **2010**, *11*, 700−704.

DOI: 10.1021/acsami.5b04334
ACS Appl. Mater. Interfaces 2015, 7, 18379−18386

(30) Sakurai, T.; Toyoshima, S.; Kitazume, H.; Masuda, S.; Kato, H.; Akimoto, K. Influence of Gap States on Electrical Properties at Interface between Bathocuproine and Various Types of Metals. *J. Appl. Phys.* **2010**, *107*, 043707.
(31) Hwang, J.; Wan, A.; Kahn, A. Energetics of Metal-Organic Interfaces: New Experiments and Assessment of the Field. *Mater. Sci. Eng., R* **2009**, *64*, 1−31.
(32) Wang, S.; Sakurai, T.; Kuroda, R.; Akimoto, K. Energy Band Bending Induced Charge Accumulation at Fullerene/Bathocuproine Heterojunction Interface. *Appl. Phys. Lett.* **2012**, *100*, 243301.
(33) Grossiord, N.; Kroon, J. M.; Andriessen, R.; Blom, P. W. M. Degradation Mechanisms in Organic Photovoltaic Devices. *Org. Electron.* **2012**, *13*, 432−456.
(34) Lee, S.-H.; Seo, J.-W.; Lee, J.-Y. Stable Inverted Small Molecular Organic Solar Cells Using a p-Doped Optical Spacer. *Nanoscale* **2015**, *7*, 157−165.
(35) Könenkamp, R.; Priebe, G.; Pietzak, B. Carrier Mobilities and Influence of Oxygen in C_{60} Films. *Phys. Rev. B: Condens. Matter Mater. Phys.* **1999**, *60*, 11804−11808.
(36) Tapponnier, A.; Biaggio, I.; Gunter, P. Ultrapure C_{60} Field-Effect Transistors and the Effects of Oxygen Exposure. *Appl. Phys. Lett.* **2005**, *86*, 112114.
(37) Proctor, C. M.; Kim, C.; Neher, D.; Nguyen, T. Q. Nongeminate Recombination and Charge Transport Limitations in Diketopyrrolopyrrole-Based Solution-Processed Small Molecule Solar Cells. *Adv. Funct. Mater.* **2013**, *23*, 3584−3594.
(38) Maurano, A.; Hamilton, R.; Shuttle, C. G.; Ballantyne, A. M.; Nelson, J.; O'Regan, B.; Zhang, W.; McCulloch, I.; Azimi, H.; Morana, M. Recombination Dynamics as a Key Determinant of Open Circuit Voltage in Organic Bulk Heterojunction Solar Cells: A Comparison of Four Different Donor Polymers. *Adv. Mater.* **2010**, *22*, 4987−4992.
(39) Credgington, D.; Hamilton, R.; Atienzar, P.; Nelson, J.; Durrant, J. R. Non-Geminate Recombination as the Primary Determinant of Open-Circuit Voltage in Polythiophene:Fullerene Blend Solar Cells: An Analysis of the Influence of Device Processing Conditions. *Adv. Funct. Mater.* **2011**, *21*, 2744−2753.
(40) Gupta, V.; Kyaw, A. K. K.; Wang, D. H.; Chand, S.; Bazan, G. C.; Heeger, A. J. Barium: An Efficient Cathode Layer for Bulk-Heterojunction Solar Cells. *Sci. Rep.* **2013**, *3*, 1965.
(41) Xu, M.-F.; Cui, L.-S.; Zhu, X.-Z.; Gao, C.-H.; Shi, X.-B.; Jin, Z.-M.; Wang, Z.-K.; Liao, L.-S. Aqueous Solution-Processed MoO_3 as an Effective Interfacial Layer in Polymer/Fullerene Based Organic Solar Cells. *Org. Electron.* **2013**, *14*, 657−664.
(42) Qin, P.; Fang, G.; Cheng, F.; Ke, W.; Lei, H.; Wang, H.; Zhao, X. Sulfur-Doped Molybdenum Oxide Anode Interface Layer for Organic Solar Cell Application. *ACS Appl. Mater. Interfaces* **2014**, *6*, 2963−2973.
(43) Shockley, W.; Read, W., Jr Statistics of the Recombinations of Holes and Electrons. *Phys. Rev.* **1952**, *87*, 835.
(44) Cowan, S. R.; Roy, A.; Heeger, A. J. Recombination in Polymer-Fullerene Bulk Heterojunction Solar Cells. *Phys. Rev. B: Condens. Matter Mater. Phys.* **2010**, *82*, 245207.
(45) McNeill, C. R.; Hwang, I.; Greenham, N. C. Photocurrent Transients in All-Polymer Solar Cells: Trapping and Detrapping Effects. *J. Appl. Phys.* **2009**, *106*, 024507.
(46) Li, Z.; Lakhwani, G.; Greenham, N. C.; McNeill, C. R. Voltage-Dependent Photocurrent Transients of PTB7: $PC_{70}BM$ Solar Cells: Experiment and Numerical Simulation. *J. Appl. Phys.* **2013**, *114*, 034502.

DOI: 10.1021/acsami.5b04334
ACS Appl. Mater. Interfaces 2015, 7, 18379−18386